Manuscript 1MOrD1-05 submitted to CEC/ICMC Proceedings in AIP Conference Proceedings

Stress-induced martensitic transformation during tensile test of full-size TF conductor jacket tube at 4.2 K

H. H. Yang[a,b], Z. X. Wu[a], C. J. Huang[a], R. J. Huang[a], S.P. Li[a,b] and L. F. Li[a]

[a]*Key Laboratory of Cryogenics, Technical Institute of Physics and Chemistry, Chinese Academy of Sciences, Beijing, 100190, P.R. China*
[b]*University of Chinese Academy of Sciences Beijing, 100049, P.R. China*

Abstract. The toroidal-field (TF) conductor jacket of the International Thermonuclear Experimental Reactor (ITER) is made of modified 316LN stainless steel, which requires post-aging treatments at 650 ℃ for 200 h to produce Nb_3Sn superconducting materials in the final stage. Due to the high electromagnetic forces arising during magnet operation, higher mechanical properties of the jacket materials at cryogenic temperatures are required. In our work, mechanical properties of the full-size TF conductor jacket tube were investigated, which satisfied the ITER IO requirements. Stress-induced martensitic transformation mechanism during tensile test of the conductor jacket material at 4.2 K was characterized by means of in-situ temperature dependent XRD, vibrating sample magnetometer (VSM), and this in conjunction with transmission electron microscopy (TEM). The tensile behavior related to the amount of stress-induced phase transformation at cryogenic temperature was also discussed.

Keywords: ITER, TF conductor jacket, Modified 316 LN, Cryogenic, Martensitic transformation

PACS:

INTRODUCTION

The toroidal-field (TF) magnet coils for ITER are made of Nb_3Sn-type superconducting cable-in-conduit conductors (CICCs) due to the requirement of high magnetic field [1]. The conductor needs special qualifications because it has to go through several processing steps to form the final superconducting coil, such as compaction, stretching and long-term aging treatment (AT) after inserting the superconducting cable into the jacket. Modified austenitic 316LN stainless steel (SS) attracts a lot of attention and has been chosen as the TF conductor jacket material, because of its high toughness, relatively high strength, high Young's modulus, low magnetic permeability and relative ease of manufacturing process. The CICCs are operated at 4.2 K, it is therefore necessary to evaluate the mechanical properties at low temperature [2].

Since both the cold work and the long-term AT ineluctably reduce the ductility of the modified 316LN SS at cryogenic temperature, the initial requirement on elongation for TF jacket is difficult to achieve. It has been proved that applying the alternative way to optimize the solution anneal treatment of the modified 316LN SS at 1100 ℃ can enhance the elongation at fracture [3].

The TF coils are practically non-repairable. Deformation accumulated during tensile test can induce transformation of γ-austenite to α'-martensite by movement of dislocations through slip [4]. Extensive work has been done to investigate the mechanical behavior of the 316LN SS after compaction and aging treatment [2, 5, 6]. However, a detailed study on the performance change of the base full-size TF conductor jacket after tensile tests at low temperature is lacking. There is a difference in the structural characteristics and formation process along the tube. The purpose of this work is to gain insight in the true mechanical performance and phase transformation of the cold-worked and aged TF conductor jacket. XRD results show that the austenitic parent phase (γ) has transformed to a secondary martensitic phase (α') after tensile test at 4.2 K, and generally, the site closer to the fracture gives more change. Based on the magnetic measurement (VSM), the calculated volume fraction ($V_{\alpha'}$) of α'-martensite at fracture is about 26%. The fracture morphology was also investigated by using TEM.

TABLE 1. The chemical composition of the TF conductor jacket material.

Element (wt.%)	C	Mn	Si	S	P	Ni	Cr	Mo	N	Co
Product analysis	0.014	1.39	0.35	0.001	0.008	13.56	16.45	2.33	0.158	0.01
ITER IO requirement	<0.02	<2.0	<0.75	<0.03	<0.04	11.0-14.0	16.0-18.0	2.0-3.0	0.14-0.18	<0.1

EXPERIMENTAL PROCEDURE

The seamless tube used in this study is made of the modified 316LN austenitic SS and provided by Zhejiang Jiuli Hi-Tech Metals co. Ltd.. Its chemical composition and the requirement of ITER IO are listed in TABLE 1. The final outer diameter of the conductor jacket is 43.7 mm and the wall thickness is 2.0 mm, as shown in FIGURE 1(a). After cold work, the conductor jacket was aged at 650 ℃ for a duration of 200 h in a vacuum furnace to simulate the Nb_3Sn formation process. The length of the full-size tube for tensile test is 260 mm and the gauge length is 100 mm.

The tensile test was carried out by a testing machine (MTS-SANS CMT5000), which was conducted in displacement control with a strain rate of 5×10^{-4} 1/s in accordance with ASTM E1450. The cryogenic environment was obtained through immersing the whole full-size tube into liquid helium.

The crystalline phases of the TF conductor jacket were detected by using in-situ temperature dependent X-ray diffractometer (XRD) in two different modes. In the first case, the specimen from the TF conductor jacket was examined at various temperatures (ca. 12 K, 30 K, 50 K, 100 K, 200 K and 300 K). In the second group, specimens in the form of discs with 6 mm in diameter were cut out from the tensile fractured tube parallel the longitudinal directions by wire-electrode cutting, named as site 1-5 (in FIGRUE 2), then were examined by using XRD measurement.

The coercive force is an indicator of the size and distribution of ferromagnetic α'-martensite formed in a paramagnetic austenitic matrix. Specimens (1.5 × 4 mm) for magnetic measurements were also taken from the tensile fractured tubular TF conductor jacket, with the same position as site 1-5. The magnetic measurements were performed in a vibrating sample magnetometer (VSM). During the measurements, a magnetic field (ca. ± 70000 Oe) was applied to induce a magnetization in samples up to saturation magnetization.

The morphology as well as the size of grains in the TF conductor jacket after tensile test (site 1) was performed using a transmission electron microscope (TEM) (JEOL JEM-2010 UHR) operating at 200 kV. Thin foils for TEM analysis were first cut from the tube perpendicular to the fracture, mechanically polished until it was about 30 μm in thickness. Then it was electro-polished using a twin-jet technique in a CH_3OH and HNO_3 solution (volume ratio=1:1) at a voltage of 60 V and current of 200 mA.

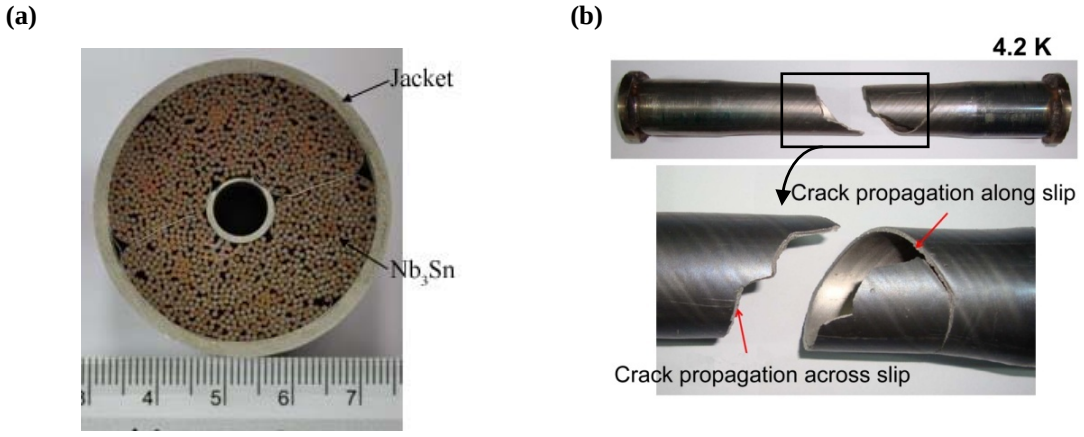

FIGURE 1. Cross section of the ITER TF condutor (a), optical images of the fractured specimens and the enlarged fracture image tested at 4.2 K (b).

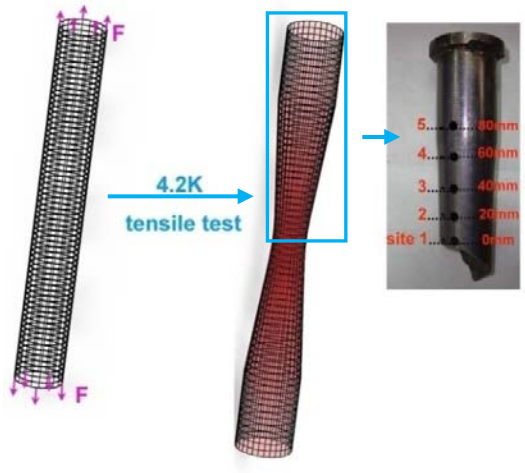

FIGURE 2. Schematic diagram of tensile test, together with the corresponding directions from site 1-5.

RESULTS AND DISCUSSION

The optical images of the fractured full-size tube are visualized in FIGURE 1(b). The tube failed not only along slip bands but also across slip bands. The appearance of macroscopic slip bands going with the occurrence of load jumps is observed clearly. Note that the initial fracture is just in the middle of the tube. ITER IO requires 0.2% offset yield strength (0.2% YS) and elongation (EL) at 4.2 K are more than 950 MPa and 20%, respectively. The 4.2 K test results present 28.8% for EL, 1100MPa for 0.2% YS and 1490 MPa for ultimate tensile strength, which are over the ITER IO requirements.

FIGURE 3 shows the results of XRD measurements. The pattern of the original (undeformed) specimen is typical for a face centered cubic lattice (fcc) structure, peaks at 2θ= 43.71°, 50.92°, 74.83°, etc., corresponding to a plane spacing of d=0.2069, 0.1792, 0.128nm, etc., respectively [7]. This demonstrates that the original material is the single γ-austenitic phase.

However, XRD patterns of specimens from site 1-5 exhibit not only γ-austenite peaks but also tensile stress induced α'-martensite peaks. Peaks at 2θ=44.56° and 82.72° of the body centered cubic (bcc) structure correspond to the plane spacing of the ferrite (d=0.2032 and 0.1171nm) [6]. Its peak intensity is strong, which demonstrates a certain amount of induced α'-martensite. The peaks of the remaining γ-austenite decrease slightly, but they do not shift. Apparently, the intensity of α' peak (mainly in (110) and (211)) has a tendency to decrease gradually. As we know, the principal requirement for high elongation appears to be continued transformation during deformation [8], which means the ongoing deformation will enhance the α'-martensite content. Considering the fact that the maximum deformation always occurred at the fracture site during the tensile test, more α'-martensite should be formed at site 1. A gradual transformation of γ into α' will occur along axis direction, shown in FIGRUE 2. However, the XRD pattern gives information just near the surface, and the $V_{\alpha'}$ value is still an issue that needs to be carefully calculated, as will be discussed later.

In order to clarify the effect of temperature on the phase transformation, XRD patterns of the original specimen were also obtained at 12 K, 20 K, 30 K, 50 K, 100 K, 200 K, and 300 K. It shows that the steel exhibits a totally γ-austenitic behavior in each spectrum, without peaks associated neither with α'-martensite nor with ε-martensite, same peaks as featured by the original specimen (the lowermost curve in FIGURE 3(a)).

As is shown in FIGURE 3(b), $M_{S'}$ is the martensite start temperature, below which some martensite forms spontaneously on cooling, whereas M_d is the temperature below which martensite begins to form with deformation [9]. The $M_{S'}$ was estimated to be < 4 K. That is why the cooling condition here (from room temperature to 12 K) does not cause any phase transformation. ΔG is defined as the free energy from M_d to $M_{S'}$. As condition of a temperature between M_d and $M_{S'}$, the applied stress or the plastic strain influence the free energy change, which act as the driving force and can cause the phase transformation. When the temperature-dependent energy (ΔG_t) decreases, less force-dependent energy (ΔG_f) is needed to induce the γ-α' phase transformation [10]. The tensile test here was operated at 4.2 K, which was thought to induce α'-martensite easily.

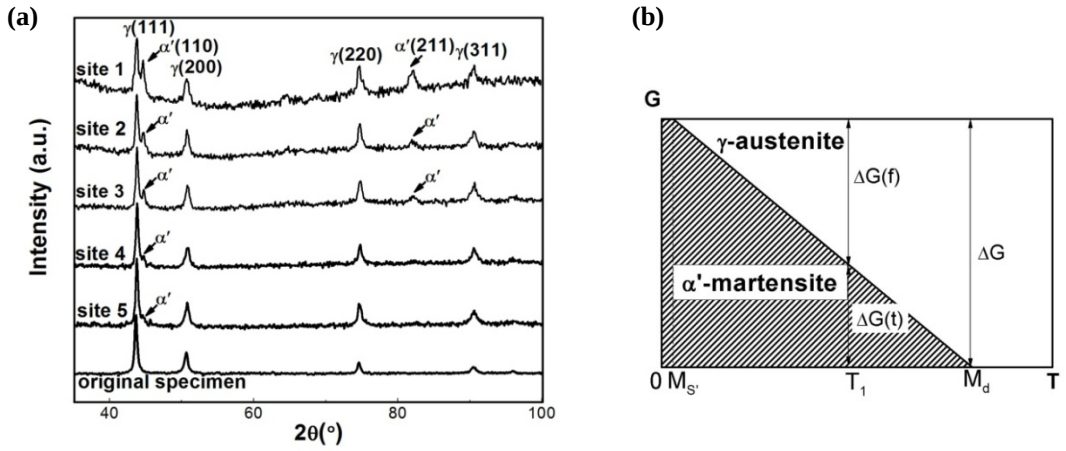

FIGURE 3. XRD patterns of specimens from site 1-5 (a), and the relationship between temperature and eneregy of strain induced α'-martensite (b).

Magnetic properties are highly sensitive to the structure of materials. In contrast to the XRD analysis, the magnetically evaluated data provide information with regard to the whole sample including both surface and the deeper interior [11].

During a magnetization loop, the magnetic field was increased from -70000 Oe up to +70000 Oe and again back to -70000 Oe. The loops yield the saturation magnetization M_s, remanent magnetization M_r, and coercive force H_c, listed in TABLE 2. All these characteristic properties are sensitive to the corresponding material changes (α'-martensite formation).

Furthermore, M_s is proportional to the volume of the ferromagnetic phase, and in specimens, where the two phases γ-austenite and α'-martensite that can coexist, α'-martensite is the only ferromagnetic one [12]. Note that each curve corresponds to a different specimen from different sites and the phase transformation is not only a function of the plastic strain but also of the local stress state [13]. While analyzing the M_s, we exclude a paramagnetic interference. Therefore, the maximum M_s value (ca. 40.2 emug/g) is for site 1, then it decreases gradually, which is in consistent with the XRD results. M_s is 5.2 emug/g for site 4, meaning only a small amount of ferromagnetic phase exists in the specimen. Site 5 gives almost sole paramagnetic behavior. Considering the fact that the distance between two adjacent sites is 20 mm, the magnetic data above suggests that the amount of α'-martensite decreases in a linearly proportional manner (FIGURE 4(a)), and α'-martensite transformation is probably considered finished at site 5. Hence, applying magnetic minor loops for the non-destructive evaluation of fracture in austenitic SS is feasible, even if a very small amount of α'-martensite is formed [14]. In addition, the saturation magnetic field of about ±1500 Oe indicates detailed hysteresis curve information in FIGURE 4(b).

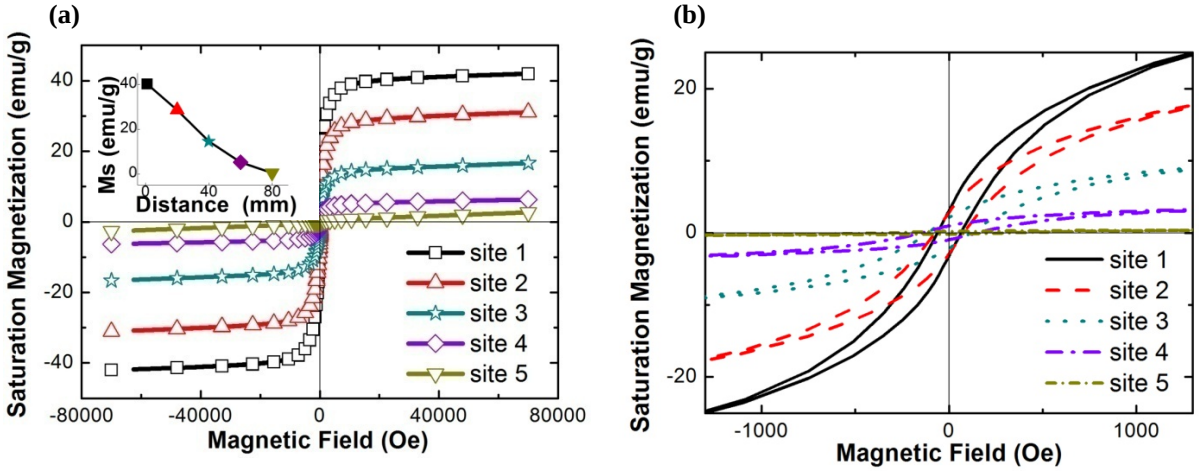

FIGURE 4. Magnetization loops, the inset shows the relationship between the M_s and distance from the fracture (a), and the enlarged magnetization loops at ±1500 Oe (b).

TABLE 2. Relative change of the saturation magnetization M_s, remanent magnetization M_r, coercive force H_c (at ±70000 Oe), and the corresponding volume fraction of α'-martensite $V_{\alpha'}$.

Specimen	M_s (emu/g)	M_r (emu/g)	H_c (Oe)	$V_{\alpha'}$ (%)
site 1	40.2	3.0	64	26.1
site 2	28.5	2.8	77	18.5
site 3	14.5	2.1	113	9.4
site 4	5.2	1.0	145	3.4
site 5	0.4	0.2	333	0.3

The intrinsic value of M_s for the 100% α'-martensite phase is 154 emu/g [12]. Consequently, the quantification of α'-martensite can be calculated from the following equation:

$$V_{\alpha'} = \frac{M_s}{154} \quad (1)$$

where $V_{\alpha'}$ is the calculated volume fraction of α'-martensite; and M_s is the saturation magnetization of each specimen.

From TABLE 2, one can see that the $V_{\alpha'}$ of site 1 is 26.1% , meaning a big amount of structure deformation occurred under tensile test at 4.2 K for the modified 316 LN SS. The coercive force (H_c) is derived from magnetic hysteresis-loop measurements, which is a function of the distribution and α'-martensite sizes, and depends on $V_{\alpha'}$ as well. H_c would be mainly determined by α'-martensite size, because the pinning strength of the magnetic domain walls at α'-γ boundaries weakens with the volume-to surface ratio. It varies inversely from the M_s with the sites changing. At the initial stage of plastic deformation, small α'-martensite particles are nucleated around the intersection of the shear bands. As the plastic deformation progress, α'-martensite particles grow, merge with each other, and form larger clusters. When the volume fraction is low, α'-martensite particles (clusters) can be considered to be isolated ones with no interparticle interactions. Consequently, it tends to decrease with the increase in α'-martensite volume fraction, reflecting an increase in the particle (cluster) size. This trend was also observed previously in AISI 304 steel [15]. In short, the magnetic results reconfirm the phase transformation, and the induced α'-martensite volume fraction can be quantified by magnetization saturation measurements.

The bright-field images of specimens after tensile test were investigated by TEM and are shown in FIGURE 5. The shear-band intersection is clear and straight, in FIGURE 5(a), with pronounced deformation, which is a commonly known as α'-martensite nucleation site and it is referred as strain induced α'-martensite. Corresponding selected area electron diffraction (SAED) patterns analyses, taken from the encircled region with the TEM micrographs, are inset in FIGURE 5(a). Many overlapping bands of thin plates are observed on {111} planes, from lower right side to upper left side direction in FIGURE 5(b). FIGURE 5(c) shows the deformed twins. Furthermore, FIGURE 5(d) identifies the presence of the lenticular like phase is also clearly identified, which is the characteristic α'-martensite structure.

Thus, in this study, intersections of deformation bands, dislocation channels and/or twins on {111} planes, have been shown to be favorable sites, which can promote the generation of α'-martensite phase. This is because α'-martensite is reported to form at intersection between two micro shear-bands, and the shear bands can be mechanical twins, dense stacking faults or twin boundaries [16]. It is also evident from the TEM bright field and dark field images that in association with formation of strain induced α'-martensite, large numbers of dislocations are generated.

CONCLUSIONS

The tensile property of the ITER TF conductor jacket was investigated at 4.2 K, and the yield strength and elongation satisfy ITER IO requirements. The induced α'-martensite phase has been identified by the XRD patterns for the specimens after tensile test, which has been additionally discussed that with decreasing the temperature, less external energy is needed to induce the γ-α' phase change. VSM data provides information with regard to the whole sample including both surface and deeper interior. The maximum volume fraction of α'-martensite phase is about

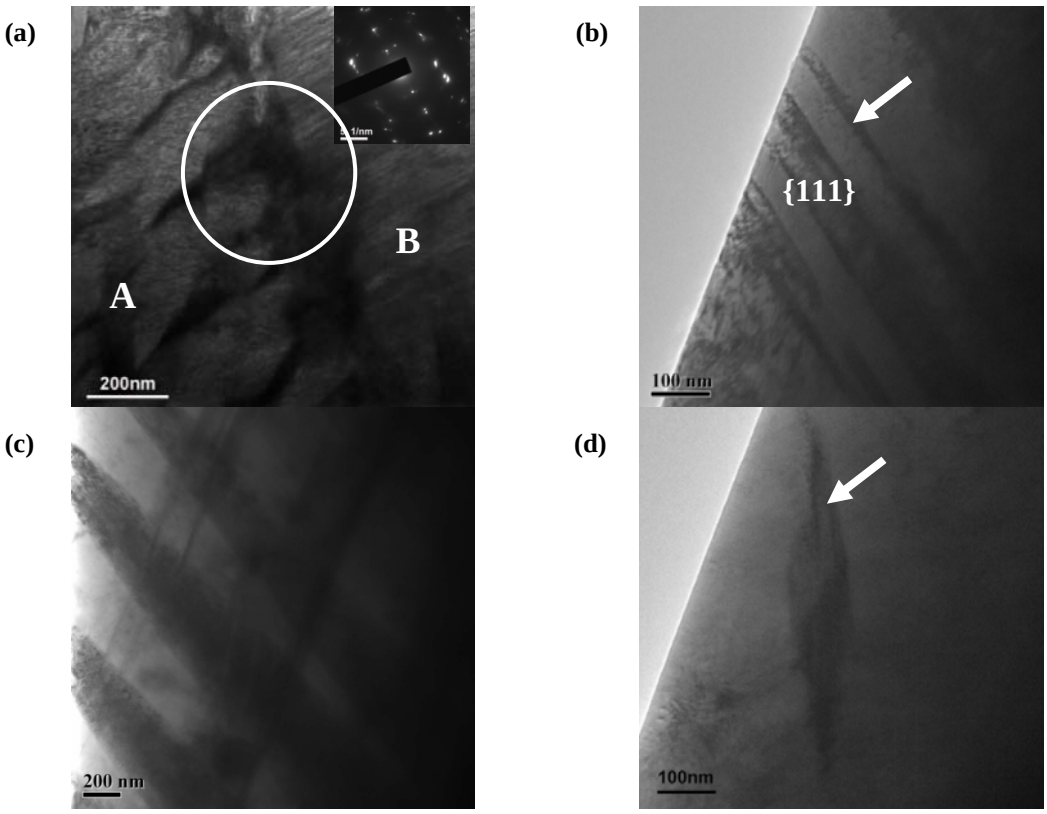

FIGURE 5. TEM images of the specimen as site 1 show shear-band intersection (a), dislocation shear bands (b) and twins (c), lenticular like α'-martensite phase (d).

26% and a gradual transformation of γ into α' occurs parallel the longitudinal direction. Overall microanalysis reveals intersections of deformation bands, dislocation channels and twins on {111} plane as the favorable sites can promote the generation of α'-martensite phase.

ACKNOWLEDGEMENTS

This work was supported by the National Magnetic Confinement Fusion Science Program of China (2011GB112004) and National Natural Sciences Foundation of China (grant No.51077123, 51177163).

REFERENCES

1. K. Hamada, Y. Takahashi, I. Takaaki, Y. Nunoya, *Fusion Eng. Des.,* **86**, pp. 1506-1510 (2011).
2. J. Qin, Y. Wu, K.-P. Weiss, Z. Wu, L. Li , *Cryogenics,* **52**, pp. 336-339 (2012).
3. C.J. Huang, Z.X. Wu, R.J. Huang, J.W. Li, S.F. Li, L.F. Li, , *24-ICMC*, pp. 909-912 (2012).
4. B.R. Kumar, B. Mahato, R. Singh, *Metall. Mater. Trans. A,* **38A**, pp. 2085-2094 (2007).
5. K.-P. Weiss, A. Ehrlich, A. della Corte, A. Vostner, *Adv. Cryog. Eng.*, **56**, pp. 3-8 (2010).
6. S.H. Park, J.Y. Kim, W.W. Park, H. Choi, Y.J. Ma, *Ieee T Appl. Supercon.,* **22**, pp. (2012).
7. Z.W. Yu, X.L. Xu, L. Wang, J.B. Qiang, *Surf. Coat. Technol.,* **153**, pp. 125-130 (2002).
8. S.S. Hecker, M.G. Stout, K.P. Staudhammer, *Metall. Mater. Trans. A,* **13**, pp. 619-626 (1982).
9. P.L. Mangonon, G. Thomas, *Metall. Trans.,* **1**, pp. 1577-& (1970).
10. J.W. Kim, T.S. Byun, *J. Nucl. Mater.,* **396**, pp. 1-9 (2010).
11. B.N. Mordyuk, G.I. Prokopenk, M.A. Vasylyev, *Metall. Mater. Trans. A,* **458**, pp. 253-261 (2007).
12. K. Mumtaz, S. Takahashi, J. Echigoya, Y. Kamada, *J. Mater. Sci.,* **39**, pp. 1997-2010 (2004).
13. M. Sitko, B. Skoczen*, Int J Solids Struct.,* **49**, pp. 613-634 (2012).
14. M. Niffenegger, H.J. Leber, *J. Nucl. Mater.,* **377**, pp. 325-330 (2008).
15. S.S.M. Tavares, J.M. Neto, M.R. da Silva, *Mater Charact,* **59**, pp. 901-904 (2008).
16. A. Das, S. Tarafder, *Int. J. Plast.,* **25**, pp. 2222-2247 (2009).